NACA TN 4087

NATIONAL ADVISORY COMMITTEE FOR AERONAUTICS

TECHNICAL NOTE 4087

DROP-SIZE DISTRIBUTION FOR CROSSCURRENT BREAKUP OF LIQUID JETS IN AIRSTREAMS

By Robert D. Ingebo and Hampton H. Foster

Lewis Flight Propulsion Laboratory
Cleveland, Ohio

Washington
October 1957

NATIONAL ADVISORY COMMITTEE FOR AERONAUTICS

TECHNICAL NOTE 4087

DROP-SIZE DISTRIBUTION FOR CROSSCURRENT BREAKUP OF LIQUID JETS IN AIRSTREAMS

By Robert D. Ingebo and Hampton H. Foster

4453

CN-1

SUMMARY

Drop-size-distribution data were obtained for liquid jets atomized by cross-stream injection from simple orifices into high-velocity airstreams. A high-speed camera and a sampling technique were combined to obtain data over ranges of injector, liquid, and airstream variables. The volume-median drop diameter D_{30} was calculated using the Rosin-Rammler, the log-probability, and the Nukiyama-Tanasawa distribution expressions. By means of dimensional analysis, the following empirical expression was obtained in correlating the ratio of the volume-median drop diameter to orifice diameter D_{30}/D_o with the Weber-Reynolds number ratio We/Re:

$$D_{30}/D_o = 3.9(We/Re)^{0.25}$$

In the preceding equation, $We = \sigma/\rho_s D_o V_s^2$ and $Re = D_o V_s/\nu$ where σ and ν are the surface tension and kinematic viscosity, respectively, of the liquid, and V_s and ρ_s are the free-stream velocity and density, respectively, of the air. A similar expression was obtained for the maximum drop diameter D_{max} in each spray.

$$D_{max}/D_o = 22.3(We/Re)^{0.29}$$

From these expressions, the following modified Nukiyama-Tanasawa expression was derived for drop-size distribution:

$$\frac{dR}{dD} = 10^6\left(\frac{We}{Re}\right)^{0.24} \frac{D^5}{D_{max}^6} e^{-22.3(We/Re)^{0.04} D/D_{max}}$$

where R is the volume fraction of drops having diameters $> D$. This expression utilizes a limiting maximum drop size and expresses drop-size distribution as a function of the dimensionless Weber-Reynolds number ratio.

INTRODUCTION

The performance of jet engines is affected by the characteristics of the injection systems (refs. 1 and 2). Up to the present time, the atomization of the liquid, and the trajectory, acceleration, and vaporization of the droplets (ref. 3) have not been specifically related to engine performance. When a better understanding of all of these factors is obtained, then designing a fuel-injection system for optimum engine performance can be accomplished on a more scientific basis.

Several investigators (refs. 4 to 7) have obtained spray drop-size-distribution data, and as a result, equations have been derived which relate mean drop diameters to factors such as surface tension and air velocity. Although physical concepts of atomization have been developed, relatively few correlations of drop-size-distribution parameters with dimensionless force ratios have been made. This can be explained by the lack of equipment and instrumentation capable of giving accurate spray drop-size-distribution data which can be quickly analyzed.

In this investigation, a high-speed camera, capable of photographing microscopic droplets traveling at high velocities in airstreams (ref. 3), was used in combination with a sampling probe technique (ref. 8). By such a combination of photographic and sampling data, spray analyses could be speeded up and a large number of sprays tested in a relatively short time. Drop-size-distribution data were obtained by using simple orifice injectors oriented normal to the airflow. The breakup of fuel jets was investigated for ranges of injector, liquid, and airstream variables. Thus, atomization of liquid jets was studied under conditions similar to those for fuel atomization in ramjet engines and afterburners. Empirical expressions were derived from a dimensional analysis of the data.

SYMBOLS

The following symbols are used in this report:

A integrated area for fuel distribution plot

a mean diameter notation

b constant

C_o orifice discharge coefficient

c mean diameter notation

D droplet diameter, cm or microns

4453

D_o	injector-orifice diameter, cm
$\overline{D}$	constant (eq. (2)), cm
D^*	constant (eq. (1)), cm
D_{30}	volume-median droplet diameter defined by the general expression $(D_{ac})^{a-c} = \frac{\Sigma nD^a}{\Sigma nD^c}$ which gives $D_{30} = (\Sigma nD^3/\Sigma n)^{1/3}$
l	orifice length, cm
n	number of droplets in given size range
q	constant
R	volume fraction of drops having diameters > D
Re	Reynolds number based on orifice diameter, D_oV_s/ν
V	velocity, cm/sec
We	Weber number, $\sigma/\rho_sV_s^2D_o$
x	vertical distance from injector orifice along spray centerline, in.
y	$\ln(D/D^*)$
ν	kinematic viscosity, cm^2/sec
μ	absolute viscosity, gm/cm sec
ρ	density, g/cu cm
σ	surface tension, dynes/cm

Subscripts:

l	liquid
max	observed maximum
o	orifice
s	free stream
t	total

APPARATUS AND PROCEDURE

The apparatus used to study the liquid-jet breakup in airstreams is shown in figures 1, 2, and 3 and described in detail in references 3 and 8. Velocity profiles in the 4- by 12-inch test section at the sampling station were relatively flat. For points up to within 1 inch of the walls, the variation was only between 2 and 4 percent, even at the highest air velocity. The air was preheated (250° to 900° F), when required, by a turbojet-engine combustor (fig. 1). The test liquids were isooctane (2,2,4-trimethylpentane), JP-5 fuel, water, benzene, and carbon tetrachloride. The liquid jets were directed at right angles to the airstream (fig. 2), from single plain orifices using pressurized nitrogen. The injector (fig. 3) was fabricated from an Inconel tube (diam. 1/2 in., wall, 1/16 in.) welded to the center of an Inconel plate (1/16" x 2" x 4") with the orifice at the center. The plate ends were beveled on the top side, and the orifices (0.010, 0.020, 0.030, and 0.040 in.) were drilled and reamed from the top side of the plate.

Photographs and sampling data were obtained by making vertical traverses along the spray centerline normal to the airstream and at a distance of 1±1/4 inch downstream from the injector. Vertical traverses made at distances of one inch on either side of the spray centerline showed no measurable effect of horizontal displacement on drop-size distribution. The high-speed camera, shown in figure 2 and described in reference 3, was used to obtain photomicrographs of the sprays (fig. 4). The sampling probe, shown in figure 2 and described in reference 8, was used for continuous sampling at airstream velocity. Isooctane and JP-fuel air samples of the sprays were passed through the NACA fuel-air mixture analyzer; from these data, spray-concentration profiles were determined. In the case of water sprays, a humidity meter was used to analyze the sample. Wet-bulb temperature measurements were obtained as described in reference 3 and used to determine benzene and carbon tetrachloride concentrations in the samples. Therefore, the analysis of the photographs gave droplet-size-distribution data, and the analysis of the probe samples gave data on liquid concentrations in the spray profile. Experimental test conditions and liquid properties are recorded in table I.

In the photomicrographs (fig. 4), the spray appears to be partially fractionated in the airstream inasmuch as the larger droplets tend to move out farther into the airstream than the smaller droplets because of the greater momentum of the larger droplets. Figure 5 shows typical spray-distribution curves for airstream velocities of 100, 180, and 300 feet per second. The 100-feet-per-second curve is replotted to a larger scale (fig. 6) in order to illustrate the method of analysis.

Since photomicrographs showed that the spray was partially fractionated in the airstream, the area under each spray-distribution curve was divided into area increments as shown in figure 6. Droplet counts were made for

each increment and combined by means of sampling probe data to obtain the mean drop diameter D_{30} as described in appendix A. Since the incremental areas contained size ranges considerably smaller than the overall size range, relatively few droplet measurements were made without incurring large statistical errors (i.e., > 3 percent). Also, the volume fraction of a given size in the entire spray was not determined directly by total droplet count. Instead, liquid concentrations were obtained from the sampling probe data and used in the final calculation of volume fractions. Thus, a relatively rapid method of size-distribution analysis
4453 was developed by combining the photographic and sampling techniques.

RESULTS AND DISCUSSION

The log-probability, Rosin-Rammler, and Nukiyama-Tanasawa expressions for size distribution were used to determine the mean drop diameter D_{30} for all of the experimental data in table I. A sample calculation of D_{30} is given in appendix A. Also, experimental data and calculated values for each distribution equation are given in table II for three airstream-velocity conditions. The log-probability expression

$$1 - R = \frac{\delta}{\sqrt{\pi}} \int_{-\infty}^{\delta y} e^{-\delta^2 y^2} \, dy \tag{1}$$

where $y = \ln(D/D^*)$, and δ is a constant used to plot data as shown in figure 7(a). Equation (1) predicts the probable existence of infinite-size drops whereas a maximum drop size was observed for each spray. Figure 7(a) shows that the data do not fall on single straight-line plots. Instead, curves were obtained which asymptotically approached a maximum size and make the determination of D_{30} quite difficult (i.e., $\delta \neq$ a constant).

Figure 7(b) shows a plot of the following Rossin-Rammler expression:

$$R = e^{-(D/\bar{D})^q} \tag{2}$$

Application of equation (2) for the calculation of D_{30} was also found to be very difficult since values of $q = 3$ were obtained. This difficulty arises when the slope of the plot q approaches 3, and D_{30} approaches zero. A similar result was noted in reference 7.

Best results were obtained with the Nukiyama-Tanasawa expression:

$$dR/dD = \frac{b^6}{120} D^5 e^{-bD} \tag{3}$$

Figures 7(c) and 8 show that D_{30} (as determined from eq. (3)) decreases as airstream velocity increases and is affected very little when both liquid and air temperature are increased. Even though equation (3) predicts infinitely large drops, straight-line plots were obtained for the entire distribution of sizes. Thus, equation (3) was used to calculate D_{30} for each test condition, and results are recorded in table III.

Tests were first made to determine the effect of injection conditions (liquid-jet velocity V_l, orifice discharge coefficient C_o, and the length-diameter ratio for the orifice l/D_o) on the mean drop diameter D_{30}. A sample of results is given in the following table for three values of airstream velocity V_s and a constant orifice diameter D_o of 0.02 inch. Airstream temperature and static pressure were approximately constant at 90° F and 29.3 inches of mercury, respectively.

V_l, ft/sec	C_o	l/D_o	D_{30}
V_s, 300 ft/sec			
182	0.87	1.00	32
80	.86	1.00	31
84	.89	4.65	33
V_s, 180 ft/sec			
204	0.88	4.65	47
84	.89	4.65	49
81	.77	1.00	47
V_s, 100 ft/sec			
81	0.77	1.00	69
80	.86	1.00	68

These data indicate relatively little effect of liquid-jet velocity, orifice discharge coefficient, and length-diameter ratio on the mean drop diameter D_{30}. This result appeared to be explained by the fact that the force of the airstream was normal to the liquid jet. Therefore, the only remaining injector variable to be considered is the orifice diameter D_o. The effect of this variable was then studied together with liquid properties and airstream conditions with the aid of dimensional analysis.

The mean drop diameter D_{30}, produced by cross-stream breakup of liquid jets in airstreams, is to be considered a function of the orifice diameter, liquid properties, and airstream conditions. Then the following expression is obtained:

$$D_{30} = \varphi(D_o,\rho_l,V_s,\sigma,\mu_l,\rho_s,\mu_s) \tag{4}$$

By rewriting equation (4), there results

4453

$$D_{30} = \alpha(D_o)^a(\rho_l)^b(V_s)^c(\sigma)^d(\mu_l)^e(\rho_s)^f(\mu_s)^g \tag{5}$$

where α is a proportionality constant. By means of dimensional analysis (appendix B) we obtain

$$\frac{D_{30}}{D_o} = \alpha\left(\frac{\sigma}{D_o\rho_l V_s^2}\right)^d \left(\frac{\mu_l}{D_o\rho_l V_s}\right)^{g+e} \left(\frac{\rho_s}{\rho_l}\right)^f \left(\frac{\mu_s}{\mu_l}\right)^g \tag{6}$$

which combines the seven variables assumed to influence D_{30} into four dimensionless groups.

To determine the proportionality constant α and the four exponents d, e, f, and g, the effect of airstream static pressure on D_{30} was investigated first because it appears only in the ratio ρ_s/ρ_l and has a negligible effect on μ_s. A plot of D_{30} against airstream static pressure is shown in figure 9, and the exponent f was found to be -1/4. Thus, equation (6) becomes

$$\frac{D_{30}}{D_o}\left(\frac{\rho_s}{\rho_l}\right)^{1/4} = \alpha\left(\frac{\sigma}{D_o\rho_l V_s^2}\right)^d \left(\frac{\mu_l}{D_o\rho_l V_s}\right)^{g+e} \left(\frac{\mu_s}{\mu_l}\right)^g \tag{7}$$

Airstream static pressure was not treated further as a separate variable.

The exponent d was determined by making tests with $(\mu_l/D_o\rho_l V_s)$ held approximately constant at several constant values of the viscosity ratio μ_s/μ_l and by varying the remaining groups. A plot of these data are shown in figure 10. In figure 10 a single straight-line plot is obtained which gives the exponent d a value of 1/4. The exponent g is approximately zero since no appreciable effect was observed when μ_s/μ_l was varied by a factor of 3.

Thus, equation (7) becomes

$$\frac{D_{30}}{D_o}\left(\frac{D_o \rho_s V_s^2}{\sigma}\right)^{1/4} = \alpha\left(\frac{\mu_l}{D_o \rho_l V_s}\right)^e = \alpha\left(\frac{\nu}{D_o V_s}\right)^e \tag{8}$$

where $(\sigma/D_o \rho_s V_s^2)$ is commonly referred to as the Weber number or the ratio of surface tension to the turbulent momentum-transfer force of the airstream. The group $(D_o V_s/\nu)$ is actually a liquid-film Reynolds number. Since the effect of air viscosity was found negligible, liquid-film resistance appeared to control the breakup process. Also, both the Weber and Reynolds numbers were based on the orifice diameter D_o as the characteristic length, and the velocity difference or relative velocity in each case is the airstream velocity V_s for cross-stream injection.

Thus, equation (8) may be rewritten as

$$\frac{D_{30}}{D_o} We^{-1/4} = \alpha\ Re^{-e} \tag{9}$$

A total of 43 tests were completed, recorded in table III, and plotted in figure 11. Results showed that $e = 1/4$, and from figure 12 it was found that $\alpha = 3.9$.

Substitution of values for e and α into equation (9) gives

$$\frac{D_{30}}{D_o} = 3.9(We/Re)^{0.25} \tag{10}$$

A comparison of equation (10) with results obtained from other methods of atomization is given in table IV.

If the maximum drop diameter D_{max} is also assumed to be a function of the properties given in equation (4), from dimensional analysis and figure 13, the result is that

$$\frac{D_{max}}{D_o} = 22.3(We/Re)^{0.29} \tag{11}$$

Thus, empirical expressions were obtained which gave relations between the mean drop diameter D_{30}, or maximum drop diameter D_{max} and the Weber-Reynolds number ratio.

The Nukiyama-Tanasawa distribution expression (eq. (3)) does not recognize the existance of a maximum drop size in a spray. However, by determining a relation between D_{30} calculated by equation (11) and the maximum drop diameter D_{max}, a modified expression for size distribution can be obtained. By combining equations (10) and (11), the following equation is obtained:

$$\frac{D_{max}}{D_{30}} = 5.7(We/Re)^{0.04} \tag{12}$$

which agrees with figure 14. Since $D_{30} = 3.915/b$, equation (3) may be rewritten

$$\frac{dR}{dD} = 10^6 \left(\frac{We}{Re}\right)^{0.24} \frac{D^5}{D_{max}^6} e^{-22.3\left(\frac{We}{Re}\right)^{0.04} \frac{D}{D_{max}}} \tag{13}$$

All of the drop-size-distribution data were tested using equation (13), and the results were good. A sample is shown in figure 15 where $\log \Delta R_t D_{max}^6/(\Delta D)D^5$ is plotted against D/D_{max} as calculated from tables II and III. Figure 15 shows that the data agree fairly well with the straight line predicted by equation (13). Thus, an expression was obtained which shows the effect of the maximum drop diameter and the Weber-Reynolds number ratio on the complete size distribution.

CONCLUSIONS

The breakup of liquid jets injected cross-stream into high velocity airstreams conformed reasonably well to the following modified Nukiyama-Tanasawa expression for drop-size distribution:

$$\frac{dR}{dD} = 10^6 \frac{D^5}{D_{max}^6} (We/Re)^{0.24} e^{-22.3\left(\frac{We}{Re}\right)^{0.04} \frac{D}{D_{max}}}$$

Also, the empirical expressions

$$D_{30} = 3.9\ D_o(We/Re)^{0.25}$$

and

$$D_{max} = 22.3\ D_o(We/Re)^{0.29}$$

were found to give good correlations of the observed maximum drop diameter D_{max}, or the mean drop diameter D_{30} with the orifice diameter D_o and the Weber-Reynolds number ratio.

Lewis Flight Propulsion Laboratory
National Advisory Committee for Aeronautics
Cleveland, Ohio, June 11, 1957

APPENDIX A

SAMPLE CALCULATION OF MEAN DROP DIAMETER D_{30}

The incremental volume function ΔR_i for each incremental area ΔA_i may be expressed as

$$\Delta R_i = n_i D^3 / \Sigma n_i D^3$$

In the first area increment (i = 1, table II) D equals 15, 25, 40, 50, and 65 microns. The corresponding number of drops n for each size was 0, 120, 80, 0, and 7, therefore,

4453

$$n_i D^3 = 0,\ 1.88\times10^6,\ 5.18\times10^6,\ 0,\ \text{and}\ 1.92\times10^6\ (\text{microns}^3)$$

respectively, and

$$\sum_{D=15}^{D=65} n_i D^3 = 8.98\times10^6\ (\text{microns}^3)$$

so that

$$\Delta R_i = \frac{n_i D^3}{\sum_{D=15}^{D=65} n_i D^3} = 0,\ 0.208,\ 0.578,\ 0,\ \text{and}\ 0.214$$

The volume fraction for a given drop size in an area increment is ΔR_i; ΔR_2, ΔR_3, ΔR_4, and ΔR_5 may be calculated in a similar manner.

The value of ΔR_t for a given drop size may be expressed as

$$\Delta R_t = \sum_{i=1}^{i=5} \Delta R_i \frac{\Delta A_i}{A}$$

For example, in table II, $A = \sum_{i=1}^{i=5} \Delta A_i = 0.0469$

And when D equals 15 microns,

$$\Delta R_t = \sum_{i=1}^{i=5} \Delta R_i \frac{\Delta A_i}{A} = 0 + \Delta R_2 \left(\frac{\Delta A_2}{A}\right) + 0 + 0 + 0 = 0.001\ \frac{0.01032}{0.0469} = 0.0002$$

where $\Delta A_i/A$ is the weight or volume fraction of drops for a given area increment, and ΔR_t is the total volume fraction for a given drop size in the entire spray.

The term R is defined as the volume fraction of drops having diameters > D. Thus, for D > 15 microns, R = 1, and for D > 225 microns, R = 0.0257 = ΔR_t.

The Nukiyama-Tanasawa expression

$$\frac{dR}{dD} = \frac{b^{6/\beta}}{\Gamma(6/\beta)} D^5 e^{-bD^\beta}$$

(where β is a constant) may be written as follows:

$$\log \frac{\Delta R_t}{(\Delta D) D^5} = -\frac{bD^\beta}{2.3} + \log \frac{b^6}{\beta \Gamma(6/\beta)}$$

Plots of $\log (\Delta R_t/(\Delta D)D^5)$ against D were made for all of the experimental drop-size-distribution data, and best results were obtained when $\beta = 1$. Thus, equation (3), $dR/dD = (b^6/120) D^5 e^{-bD}$, was obtained, which may be rewritten as follows:

$$\log \frac{\Delta R_t}{(\Delta D) D^5} = -\frac{b}{2.3} D + \log \frac{b^6}{120}$$

where $-(b/2.3)$ is the slope of the plot in figures 7(c) or 8. Integration of the preceding expression yields the following general expression for mean drop sizes:

$$D_{ac}^{a-c} = b^{-(a-c)} \Gamma(a + 3)/\Gamma(c + 3)$$

Thus, the equation for D_{30} (a = 3, and c = 0) becomes

$$D_{30}^3 = b^{-3} \Gamma 6/\Gamma 3$$

or

$$D_{30} = 3.915/b$$

Other mean drop diameters may be readily obtained from the general expression for mean drop sizes. In figure 6(c), the slope of the plot for V_s = 300 feet per second is

$$\text{slope} = \frac{-12.3 + 8.1}{100} = -0.042 = -\frac{b}{2.3}$$

thus,

$$D_{30} = 3.915/(2.3)(0.042) = 40.5 \text{ microns}$$

APPENDIX B

DIMENSIONAL ANALYSIS

When equation (5) is rewritten, the following expression results:

$$D_{30} = \alpha(D_o)^a(\rho_l)^b(V_s)^c(\sigma)^d(\mu_l)^e(\rho_s)^f(\mu_s)^g$$

The preceding equation is then expressed in terms of the mass-length-time system (where T is time; M, mass; and l, length) to give

$$l = \alpha(l)^a\left(\frac{M}{l^3}\right)^b\left(\frac{l}{T}\right)^c\left(\frac{M}{T^2}\right)^d\left(\frac{M}{lT}\right)^e\left(\frac{M}{l^3}\right)^f\left(\frac{M}{lT}\right)^g$$

so that for

$$\Sigma M, \qquad 0 = b + d + e + f + g$$

$$\Sigma l, \qquad 1 = a - 3b + c - e - 3f - g$$

$$\Sigma T, \qquad 0 = -c - 2d - e - g$$

which may be rewritten as

$$a = 1 - d - e - g$$

$$b = -d - e - f - g$$

$$c = -2d - e - g$$

Substitution of these values into equation (5) gives

$$\frac{D_{30}}{D_o} = \left(\frac{\sigma}{V_s^2\rho_l D_o}\right)^d\left(\frac{\mu_l}{\rho_l D_o V_s}\right)^{g+e}\left(\frac{\rho_s}{\rho_l}\right)^f\left(\frac{\mu_s}{\mu_l}\right)^g$$

which is equation (6).

REFERENCES

4453

1. Sharp, J. G.: Effects of Fuel Type on the Performance of Aero-Gas Turbine Combustion Chambers, and the Influence of Design Features. Jour. Roy. Aero. Soc., vol. 58, no. 528, Dec. 1954, pp. 813-825.

2. The Staff of the National Gas Turbine Establishment: The Correlation of Combustion Efficiency and Injector Characteristics Under Simulated Altitude Idling Conditions. Combustion Res. and Rev., Butterworths Sci. Pub. (London), 1955, pp. 53-57.

3. Ingebo, Robert D.: Vaporization Rates and Drag Coefficients for Isooctane Sprays in Turbulent Air Streams. NACA TN 3265, 1954.

4. Nukiyama, Shirō, and Tanasawa, Yasushi (E. Hope, Trans.): Experiments on the Atomization of Liquids in an Air Stream. Rep. No. 3, On the Droplet-Size Distribution in an Atomized Jet, Defence Res. Board, Dept. Nat. Defence, Ottawa (Canada), Mar. 18, 1950. (Trans. from Trans. Soc. Mech. Eng. (Japan), vol. 5, no. 18, Feb. 1939, pp. 62-67.)

5. Conroy, E. H., and Johnstone, H. F.: Combustion of Sulfur in a Venturi Spray Burner. Ind. and Eng. Chem., vol. 41, no. 12, 1949, pp. 2741-2748.

6. Longwell, J. P.: Fuel Oil Atomization. D.Sc. Thesis, M.I.T., 1943.

7. Bowen, I. G., and Joyce, J. R.: The Effects of Cone Angle, Pressure and Flow Number on the Particle Size of a Pressure Jet Atomiser. Tech. Rep. No. I.C.T./17, The Shell Petroleum Co., Ltd. (London), Mar. 15, 1948.

8. Foster, Hampton H., and Ingebo, Robert D.: Evaporation of JP-5 Fuel Sprays in Air Streams. NACA RM E55K02, 1956.

9. Turner, G. M., and Moulton, R. W.: Drop Size Distributions from Spray Nozzles. Chem. Eng. Prog., vol. 49, no. 4, Apr. 1953, pp. 185-190.

4453

TABLE I. - TEST CONDITIONS FOR CROSS-STREAM BREAKUP OF LIQUID JETS

Run	Injector orifice diameter, in.	Air-stream velocity, ft/sec	Air temperature, °F	Air pressure, in. Hg abs	Air density, lb/cu ft	Liquid jet velocity, ft/sec	Liquid temperature, °F	Liquid density, lb/cu ft	Liquid viscosity, millipoises	Surface tension, dynes/cm
Isooctane										
1	0.010	100	89	29.3	0.071	180	88	42.6	4.75	20.7
2	.020		87		.071	80	91			
3	.020		85		.071	81	94			
4	.030		88		.071	51	93			
5	.030	180	90	20	.048	76	82			
6	.040		86	29.3	.071	59	90			
7	.020		90		.071	80	93			
8			85		.071	81	94			
9			85		.071	84	88			
10			87		.071	204	86			
11	.030		87		.071	51	92			
12			87		.071	51	198	40.0	2.85	16.0
13			82		.072	54	82	42.6	4.75	20.7
14			80		.072	76	80			
15			80	50	.123	76	83			
16			82	29.3	.071	76	82			
17	.020		300		.051	83	150	40.0	2.85	16.0
18	.030		900		.029	51	200			
19	.020		900		.029	82	174			
20		300	87		.071	80	93	42.6	4.75	20.7
21			87		.071	182	82			
22			87		.071	84	94			
23	.030		85		.071	51	85			
24	.040		86		.071	58	88			
25	.030	350	900		.029	51	98			
26		352	900		.029	80	186	40.0	2.85	16.0
27		700	900		.029	42	200			
28		700	900		.029	79	150			
JP-5 Fuel										
29	0.030	180	80	29.3	0.071	54	80	51.1	15.8	28.5
30	.030	300	80	29.3	.071	54	80	51.1	15.8	28.5
Benzene										
31	0.030	352	900		0.029	53.5	150	52.0	3.7	22.6
32	.030	700	900	29.7	.029	53.5	145	52.0	3.8	23.0
Carbon tetrachloride										
33		180	86	29.3	0.071	35.5	87	99.5	8.4	25.2
34		300	86	29.3	.071	35.5	87	99.5	8.4	25.2
Water										
35	0.020	100	86	29.3	0.071	70	76	62.4	8.4	71.0
36		180	82		.071	73	90	62.4	8.4	71.0
37			900		.029	73	140	62.3	4.70	66.2
38			250		.055	72.5	140			
39			250		.055	70				
40		350	900		.029	72.5				
41		700		29.9	.029	70				
42	.030	300	84	29.3	.071	48.2	99		8.4	71.0
43		180				48.2				

TABLE II. - SAMPLE DROP-SIZE-DISTRIBUTION DATA AND CALCULATIONS FOR ISOOCTANE SPRAY

[Jet stream velocity, 51 ft/sec; jet density, 42.6 lb/cu ft; orifice diameter, 0.030 in.; downstream distance from injector, 1±1/4 in.]

(a) Run 4; airstream velocity, 100 ft/sec; air temperature, 88° F; air pressure, 29.3 in. Hg abs

Distance[a] from orifice, x, in.		0 to 1.5		1.5 to 2.1		2.1 to 2.5		2.5 to 2.9		2.9 to 3.5		ΔR_t	Volume fraction of drops having diameter > D, R	Log $\frac{1}{R}$	Log $\frac{\Delta R}{(\Delta D)D^5}$	100 (1-R)	Log D
Area increment[a], ΔA		0.00327		0.01032		0.01372		0.01413		0.00548							
Drop diameter, D, microns		n_1 (b)	ΔR_1	n_2	ΔR_2	n_3	ΔR_3	n_4	ΔR_4	n_5	ΔR_5			(c)	(d)	(e)	(e)
Range	Average																
7.5 - 20	15	0	0	60	0.001	0	0	0	0	0	0	0.0002	1.0000	0	-10.506	0	1.176
20 - 32.5	25	120	.208	575	.060	22	.003	0	0	0	0	.0285	.9997	.0001	-9.632	.03	1.398
32.5 - 45	40	81	.578	193	.082	45	.007	0	0	0	0	.0603	.9712	.0127	-10.327	2.88	1.602
45 - 57.5	50	0	0	193	.161	83	.024	15	.006	0	0	.0441	.9109	.0405	-10.948	8.91	1.699
57.5 - 70	65	7	.214	64	.117	49	.031	4	.003	3	.006	.0515	.8668	.0621	-11.450	13.32	1.813
70 - 82.5	75	0	0	23	.065	40	.039	7	.009	6	.018	.0305	.8154	.0886	-11.989	18.46	1.875
82.5 - 95	90			34	.165	52	.087	11	.024	7	.037	.0735	.7849	.1052	-12.001	21.51	1.954
95 - 107.5	100			13	.087	38	.087	10	.030	6	.044	.0589	.7114	.1479	-12.327	28.86	2.000
107.5 - 120	115			10	.100	19	.066	20	.092	3	.033	.0735	.6525	.1855	-12.534	34.76	2.060
120 - 132.5	125			5	.065	36	.161	25		4	.059	.1130	.5790	.2373	-12.528	42.10	2.097
132.5 - 145	140			2	.037	18	.113	15	.125	3	.061	.0860	.4660	.3316	-12.893	53.40	2.146
145 - 157.5	150			1	.023	10	.078	8	.082	0	0	.0523	.3800	.4202	-13.259	62.00	2.176
157.5 - 170	165			0	0	6	.062	10	.137	3	.099	.0708	.3277	.4845	-13.334	67.23	2.217
170 - 182.5	175			1	.036	9	.111	7	.114	2	.079	.0838	.2569	.5902	-13.389	74.31	2.243
182.5 - 195	190			0		5	.079	7	.146	3	.152	.0847	.1731	.7617	-13.568	82.69	2.279
195 - 207.5	200					0	0	2	.049	2	.118	.0284	.0884	1.0538	-14.148	91.16	2.301
207.5 - 220	215					0	0	0	0	4	.294	.0343	.0600	1.2224	-14.224	94.01	2.332
220 - 232.5	225					2	.0523	1	.035	0	0	.0257	.0257	1.5906	-14.448	97.43	2.352

[a]Fig. 5

[b]Number of drops n.

[c]Fig. 6(b).

[d]Figs. 6(c) and 7; ΔD = 12.5 microns.

[e]Fig. 6(a).

4453

TABLE II. - Concluded. SAMPLE DROP-SIZE-DISTRIBUTION DATA AND CALCULATIONS FOR ISOOCTANE SPRAY

[Jet stream velocity, 51 ft/sec; jet density, 42.6 lb/cu ft; orifice diameter, 0.030 in.; downstream distance from injector, 1±1/4 in.]

(b) Run 11; airstream velocity, 180 ft/sec; air density, 0.072 lb/cu ft

Distance from orifice, x, in.		0 to 1.0		1.0 to 1.9		ΔR_t	Volume fraction of drops having diameter >D, R	Log $\frac{1}{R}$	Log $\frac{\Delta R}{(\Delta D)D^5}$	100 (1-R)	Log D
Area increment, ΔA		0.01394		0.0597							
Drop diameter, D, microns		n_1	ΔR_1	n_2	ΔR_2						
Range	Average							(a)	(b)	(c)	(c)
5 - 17.5	15	950	0.045	120	0	0.0095	1.00	0	-9.000	0	1.176
17.5 - 30	25	611	.135	70	.003	.0280	.9905	.0041	-9.639	.95	1.398
30 - 42.5	40	315	.285	30	.006	.0583	.9625	.0166	-10.342	3.75	1.607
42.5 - 55	50	173	.305	170	.061	.1068	.9042	.0438	-10.563	9.58	1.699
55 - 67.5	65	38	.147	129	.101	.1095	.7974	.0983	-11.122	20.26	1.813
67.5 - 80	75	4	.024	117	.140	.1183	.6878	.1625	-11.399	31.22	1.875
80 - 92.5	90	3	.031	83	.172	.1453	.5695	.2445	-11.706	43.05	1.954
92.5 - 105	100	2	.028	66	.188	.1575	.4242	.3724	-11.900	57.58	2.000
105 - 117.5	115	0	0	33	.143	.1157	.2667	.5740	-12.337	73.33	2.060
117.5 - 130	125			21	.117	.0946	.1510	.8210	-12.606	84.90	2.097
130 - 142.5	140			4	.031	.0253	.0564	1.2484	-13.424	94.36	2.146
142.5 - 155	150			4	.038	.0311	.0311	1.5068	-13.484	96.89	2.176

(c) Run 23; airstream velocity, 300 ft/sec; air density, 0.072 lb/cu ft

Distance from orifice, x, in.		0 to 0.4		0.4 to 0.9		ΔR_t	Volume fraction of drops having diameter >D, R	Log $\frac{1}{R}$	Log $\frac{\Delta R}{(\Delta D)D^5}$	100 (1-R)	Log D
Area increment, ΔA		0.01514		0.06473							
Drop diameter, D, microns		n_1	ΔR_1	n_2	ΔR_2						
Range	Average							(a)	(b)	(c)	(c)
5 - 17.5	15	48	0.084	30	0.004	0.0187	1.000	0	-8.705	0	1.176
17.5 - 30	25	20	.162	80	.043	.0656	.9813	.0083	-9.270	1.87	1.398
30 - 42.5	40	6	.199	55	.121	.1360	.9157	.0383	-9.974	8.43	1.602
42.5 - 55	50	3	.194	36	.155	.1625	.7797	.1081	-10.381	22.03	1.699
55 - 67.5	65	1	.142	17	.161	.1573	.6172	.2096	-10.965	38.28	1.813
67.5 - 80	75	1	.219	11	.160	.1710	.4599	.3373	-11.239	54.01	1.875
80 - 92.5	90	0	0	8	.201	.1628	.2889	.5393	-11.656	71.11	1.954
92.5 - 105	100			3	.103	.0837	.1261	.8993	-12.174	87.39	2.000
105 - 117.5	115			1	.052	.0425	.0423	1.3732	-12.772	95.77	2.061

[a] Fig. 6(b).

[b] Figs. 6(c) and 7.

[c] Fig. 6(a).

4453

TABLE III. - MAXIMUM DROP SIZE D_{max}, MEAN DROP SIZE D_{30}, AND DIMENSIONLESS FORCE RATIOS

Run	D_{max}	D_{30}	Weber number, We, $\frac{\sigma}{V_s^2 \rho_s D_o}$	Reynolds number, Re, $\frac{D_o V_s}{\nu}$	We/Re	D_{30}/D_o	$\left(\frac{We}{Re}\right)^{0.25}$	$\frac{D_{max}}{D_{30}}$
Isooctane								
1	175	55	77.4×10^{-3}	11,100	6.95×10^{-6}	0.216	0.052	3.20
2	225	68	38.6	22,300	1.735	.134	.036	3.30
3	190	69	38.5	22,300	1.72	.137	.036	2.74
4	225	81	25.8	33,900	.76	.106	.020	2.79
5	175	65	11.7	60,000	.194	.0856	.021	2.68
6	190	62	5.9	80,300	.074	.0609	.010	3.07
7	150	47	11.9	40,100	.299	.0927	.020	3.18
8	140	47	11.9	40,100	.296	.0927	.023	2.97
9	150	49	11.9	40,100	.296	.0955	.023	3.09
10	140	47	11.9	40,100	.297	.0927	.023	2.97
11	150	52	7.9	60,000	.130	.0745	.019	2.64
12	140	47	6.1	93,600	.065	.0620	.016	2.96
13	140	55	7.9	60,000	.131	.0720	.019	2.56
14	140	53	7.9	60,000	.131	.0696	.019	2.64
15	140	51	4.6	60,000	.076	.0665	.017	2.76
16	140	50	7.9	60,000	.131	.0720	.019	2.80
17	140	48	12.8	64,600	.197	.0954	.021	2.89
18	165	55	15.3	94,800	.161	.0718	.020	3.01
19	150	50	25.0	58,900	.425	.0984	.025	3.00
20	100	31	4.3	66,800	.064	.0607	.016	3.24
21	90	32	4.3	66,900	.064	.0632	.016	2.21
22	90	33	4.3	66,800	.064	.0642	.016	2.75
23	115	40	2.9	101,700	.028	.0532	.013	2.84
24	115	40	2.14	133,700	.016	.0393	.011	2.84
25	115	37	4.03	198,300	.022	.0484	.012	3.12
26	100	37	4.01	184,200	.022	.0484	.012	2.70
27	60	24	1.01	366,300	.003	.0319	.007	2.47
28	60	24	1.01	366,000	.003	.0323	.007	2.44
JP-5 Fuel								
29	225	72	10.8	21,700	0.497	0.0950	0.026	3.12
30	150	55	3.9	36,200	.107	.0720	.018	2.74
Benzene								
31	125	40	5.6	184,400	0.031	0.0532	0.013	3.08
32	70	24	1.4	357,100	.004	.0319	.008	2.88
Carbon tetrachloride								
33	140	56	9.6	79,500	0.121	0.0731	0.019	2.51
34	100	36	3.5	132,500	.026	.0475	.013	2.76
Water								
35	375	103	132.1	18,500	7.150	0.2022	0.052	3.64
36	250	68	40.5	33,200	1.220	.1338	.034	3.68
37	225	71	94.7	59,300	1.590	.1393	.036	3.18
38	200	60	49.4	59,300	.835	.1192	.030	3.30
39	225	63	49.4	59,300	.835	.124	.030	3.57
40	125	42	25.0	115,300	.217	.0837	.022	2.94
41	75	25	6.1	230,600	.027	.0493	.013	3.00
42	150	50	9.8	83,000	.118	.0656	.018	3.00
43	315	85	27.1	49,700	.547	.1115	.027	3.70

TABLE IV. - COMPARISON OF EXPERIMENTAL RESULTS WITH

OTHER METHODS OF ATOMIZATION

Type of atomization	Mean drop size	Related properties and exponents	Source
Crosscurrent breakup of liquid jets	D_{30}, or $\left(\frac{\Sigma nD^3}{\Sigma n}\right)^{1/3}$	$\frac{(D_o)^{0.5}(\sigma)^{0.25}(\mu_l)^{0.25}}{(\rho_l)^{0.25}(V_s)^{0.75}(\rho_s)^{0.25}}$	Eq. (10)
Pressure type (centrifugal nozzles)	$\frac{\Sigma nD^3 \log D}{\Sigma nD^3}$	$\frac{(D_o)^{0.6}(\sigma)^{0.7}(\mu_l)^{0.2}}{(\rho_l)^{0.45}(V_l)^{0.45}}$	Ref. 9; av. for 2 nozzles
Air atomization	D_{32}, or $\frac{\Sigma nD^3}{\Sigma nD^2}$	$\frac{(\sigma)^{0.5}}{(\rho_l)^{0.5}(V_s)^{1.0}}$	Ref. 4; for high ratio of air- to liquid-volumetric flow rates

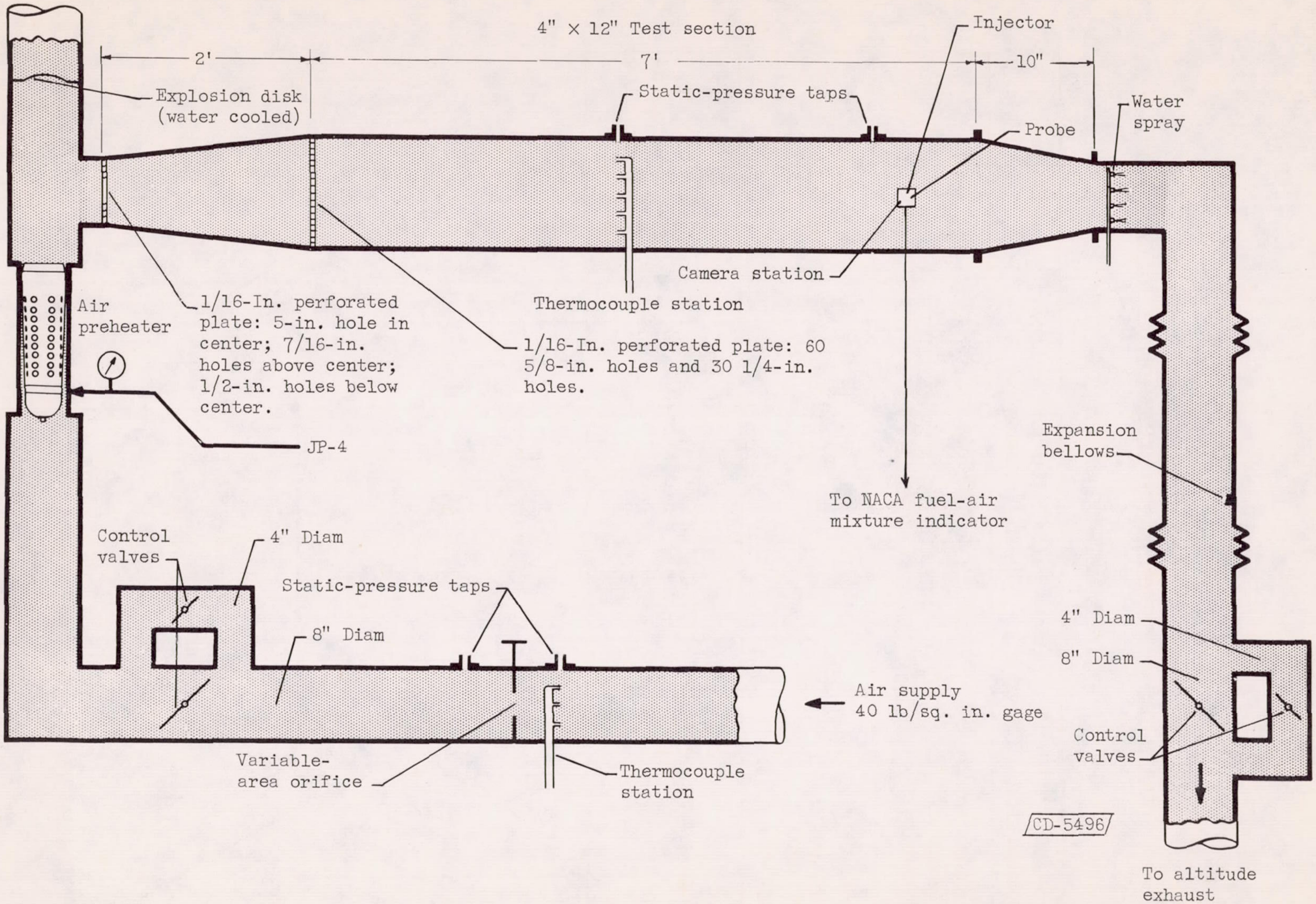

Figure 1. - Schematic drawing of test installation.

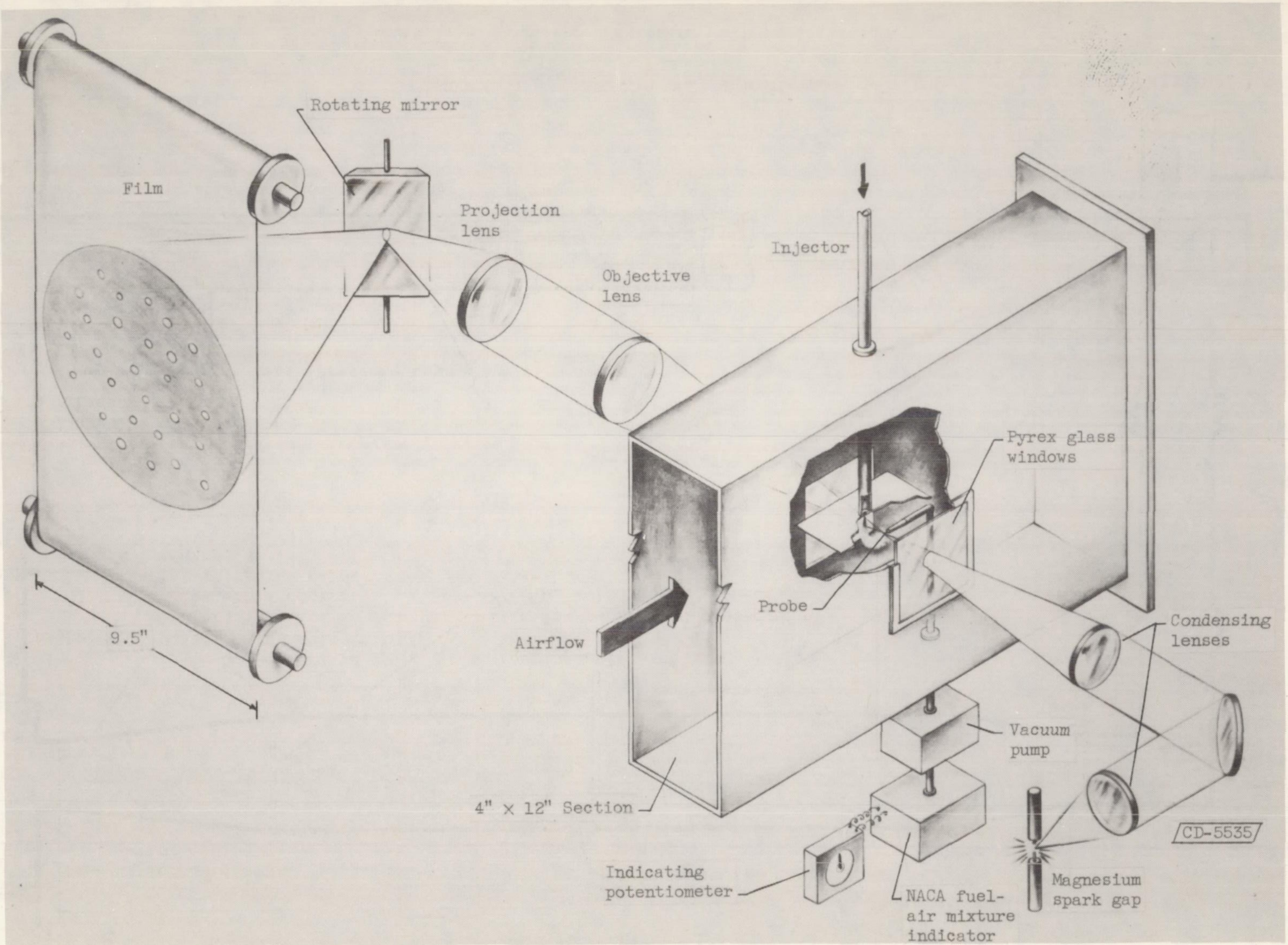

Figure 2. - Diagram of test section equipment and camera unit.

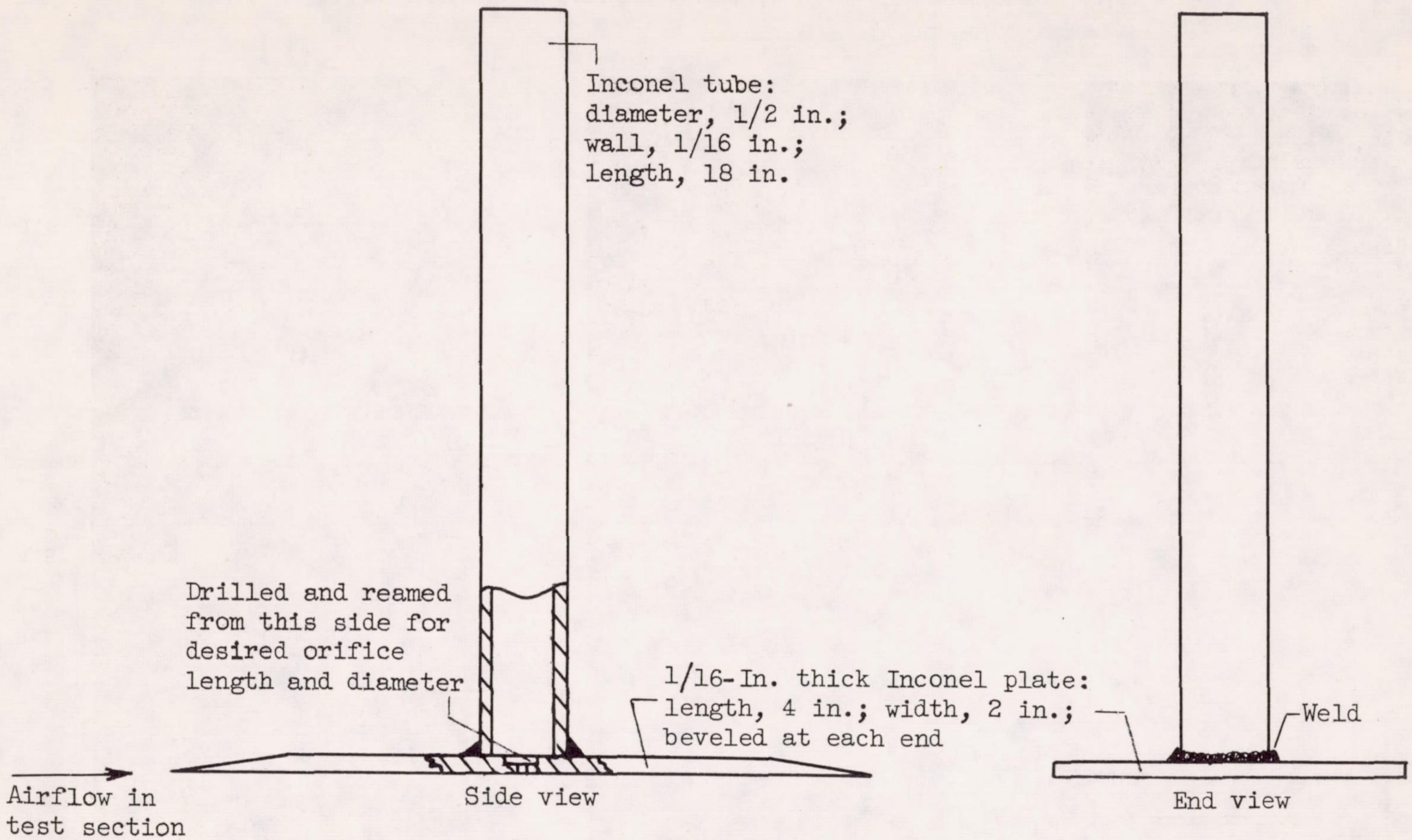

Figure 3. - Sketch of injector.

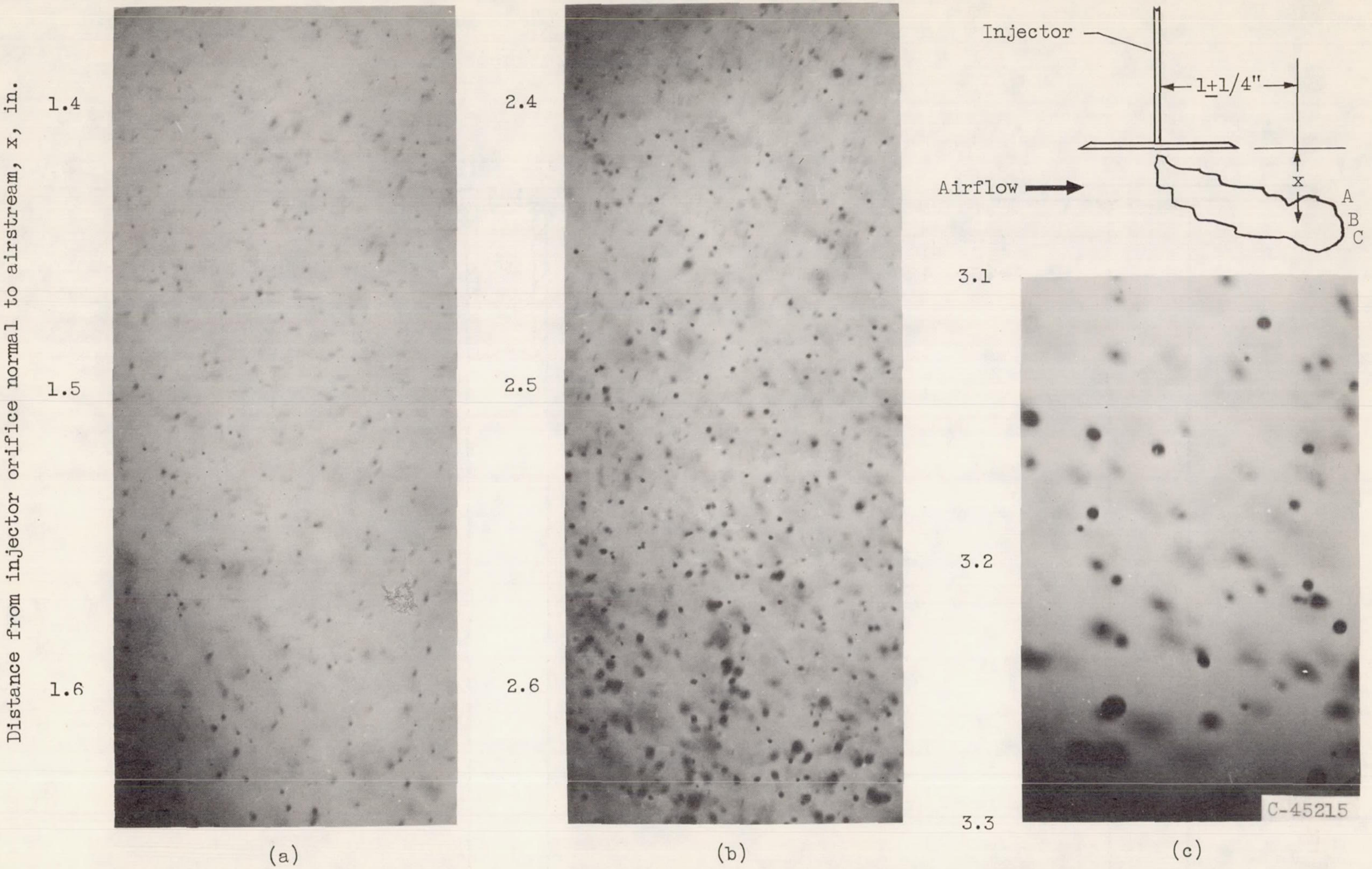

Figure 4. - Photomicrographs of isooctane spray in 100 feet per second velocity airstream. Magnification, 21:1; data, table I.

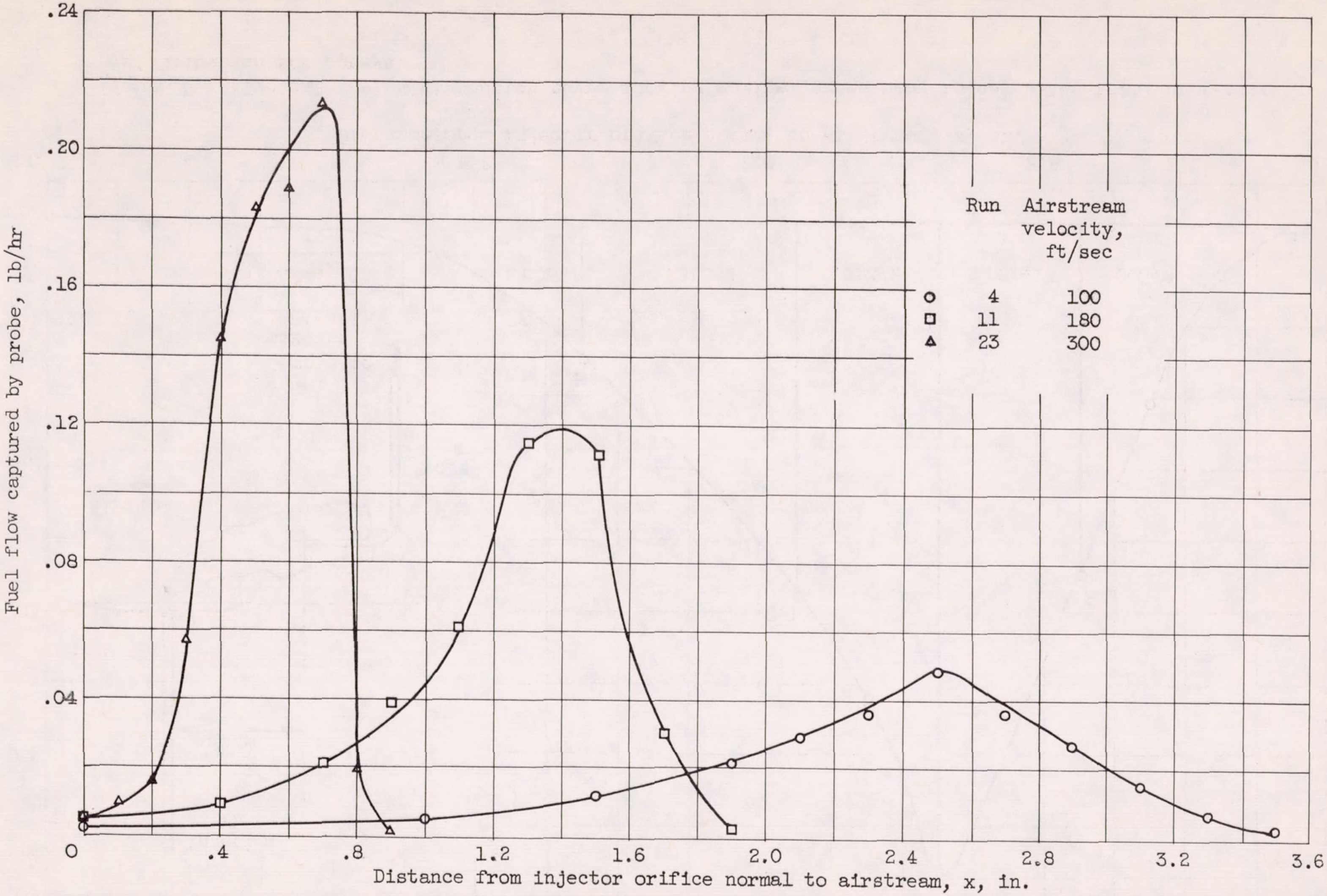

Figure 5. - Distribution of isooctane sprays normal to the airflow and 1 inch downstream from the injector. Orifice diameter, 0.030 inch; fuel jet velocity, 51 feet per second; fuel density, 42.6 pounds per cubic foot; air temperature, 86° F; air pressure, 29.3 inches of mercury absolute.

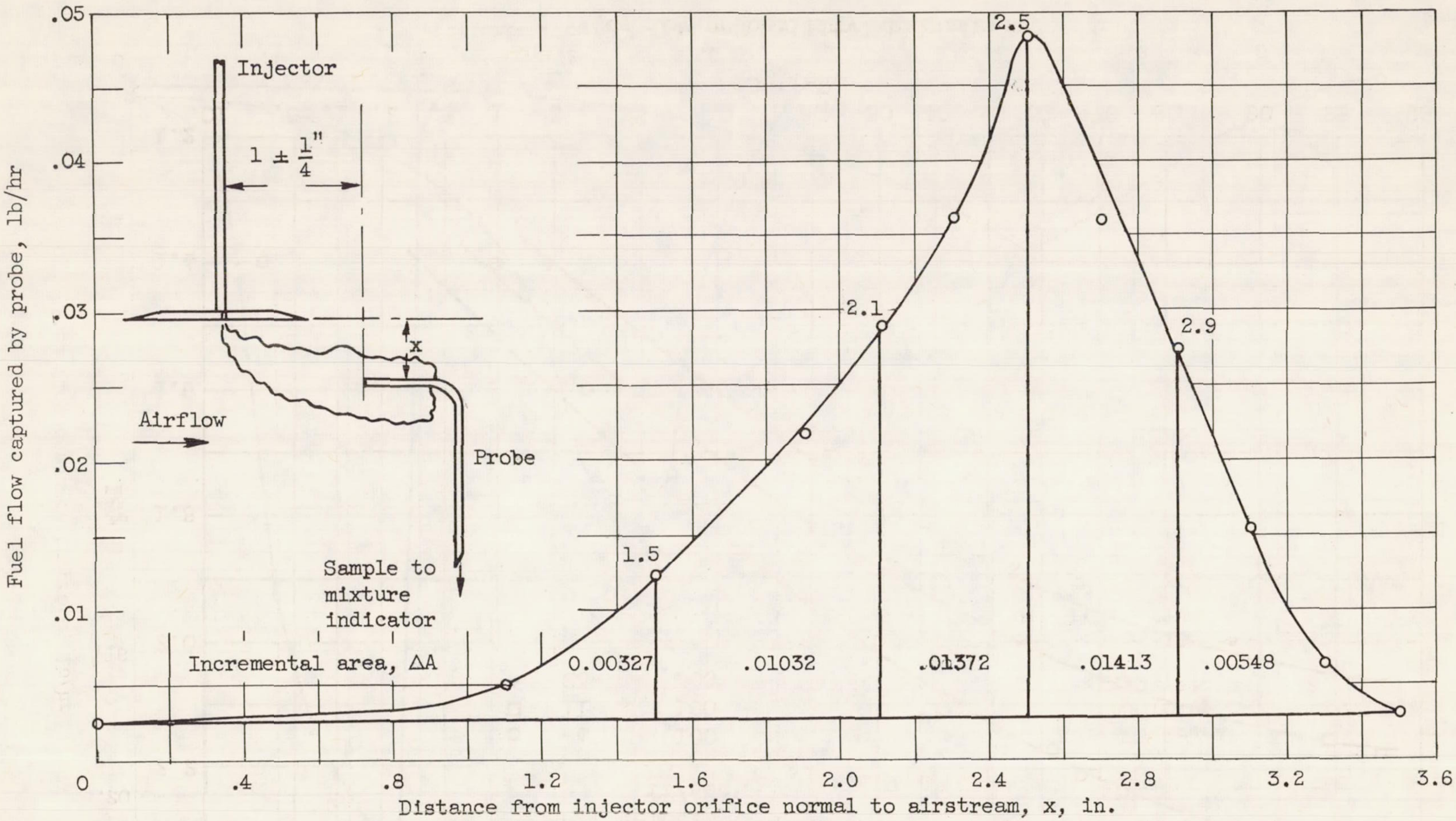

Figure 6. - Typical fuel distribution curve showing nominal areas used to calculate total drop-size distribution for sprays.

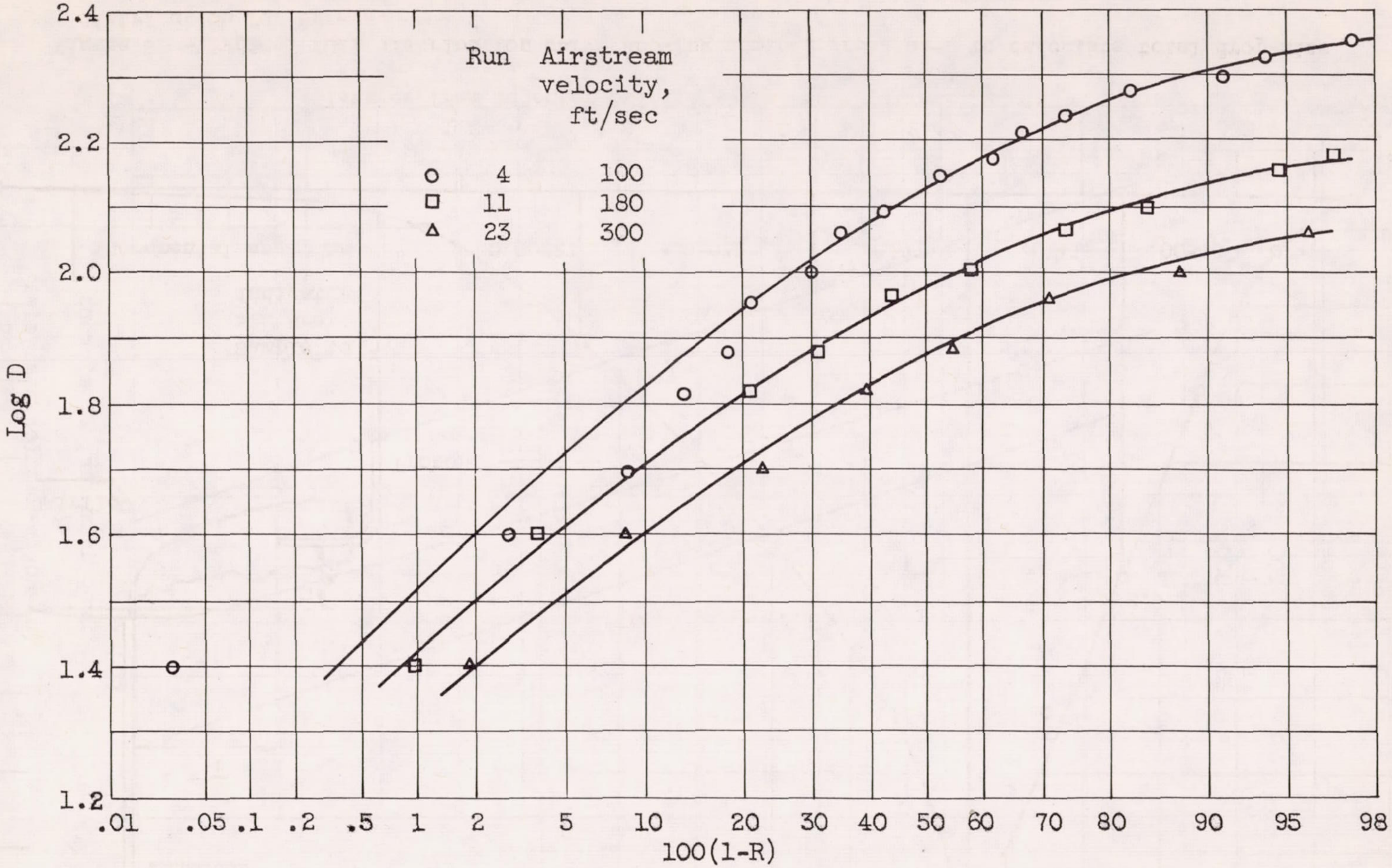

(a) Log-probability analysis.

Figure 7. - Effect of airstream velocity on atomization of crosscurrent isooctane jets.

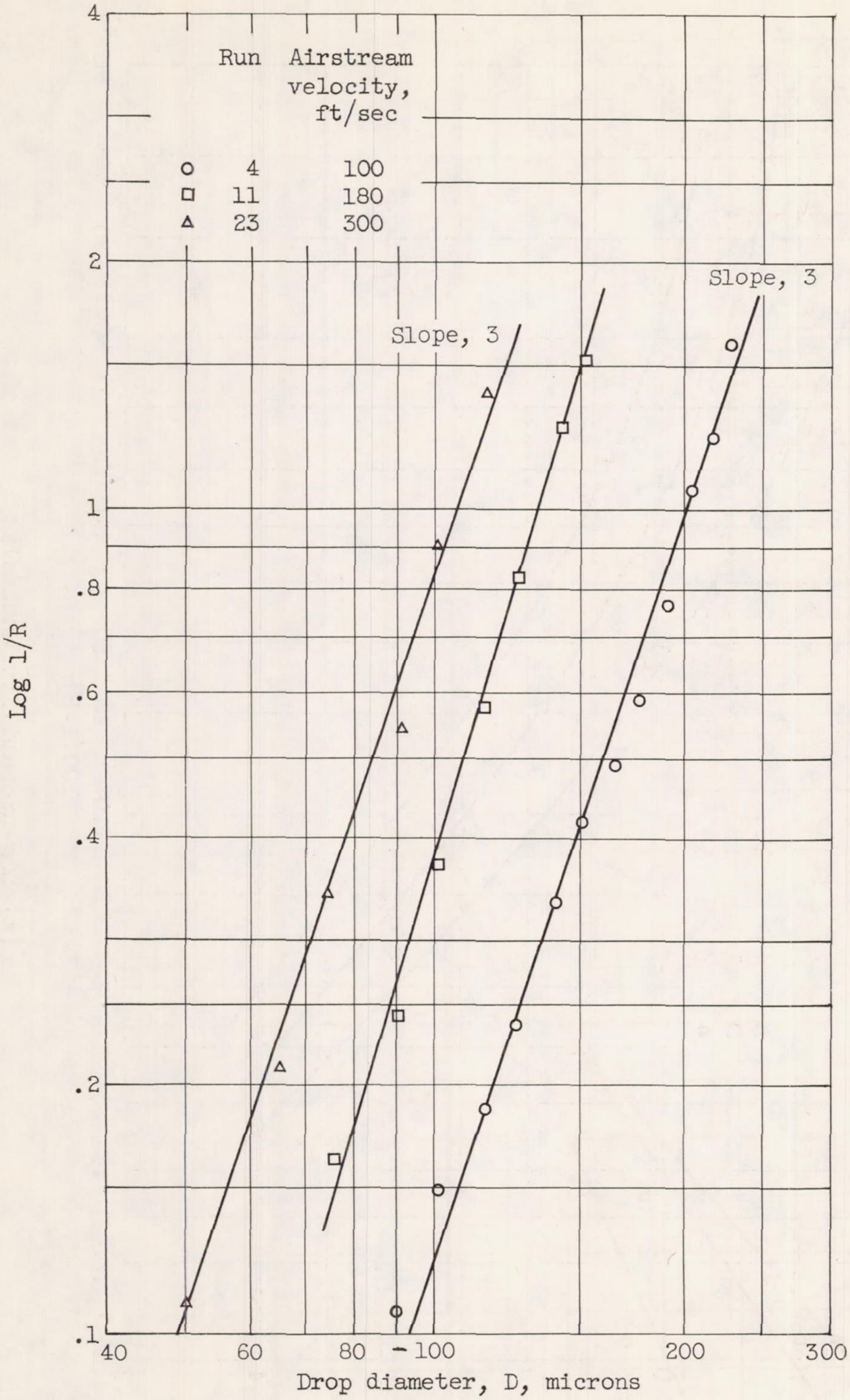

(b) Rosin-Rammler analysis.

Figure 7. - Continued. Effect of airstream velocity on atomization of crosscurrent isooctane jets.

4453

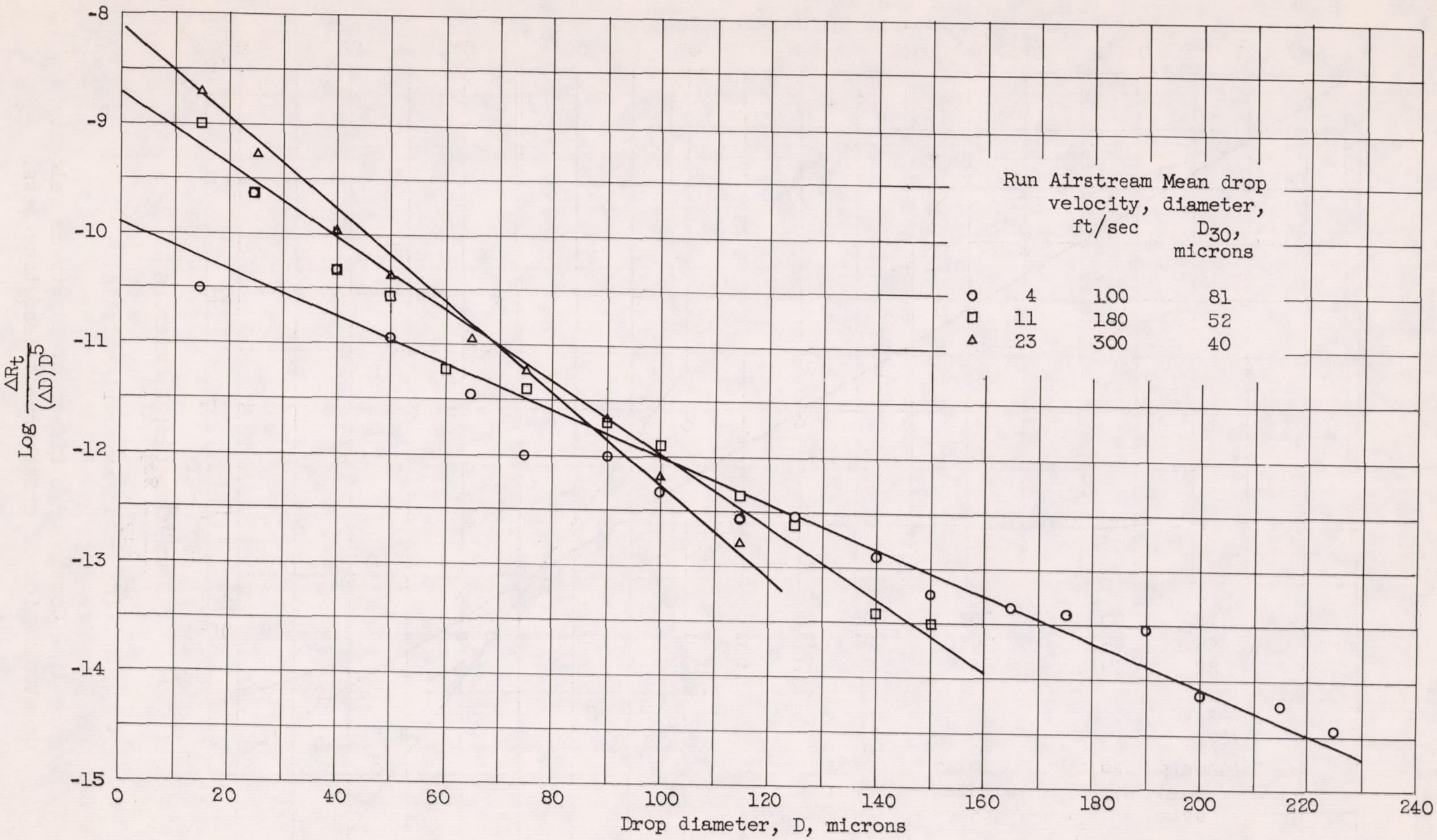

(c) Nukiyama-Tanasawa analysis.

Figure 7. - Concluded. Effect of airstream velocity on atomization of crosscurrent isooctane jets.

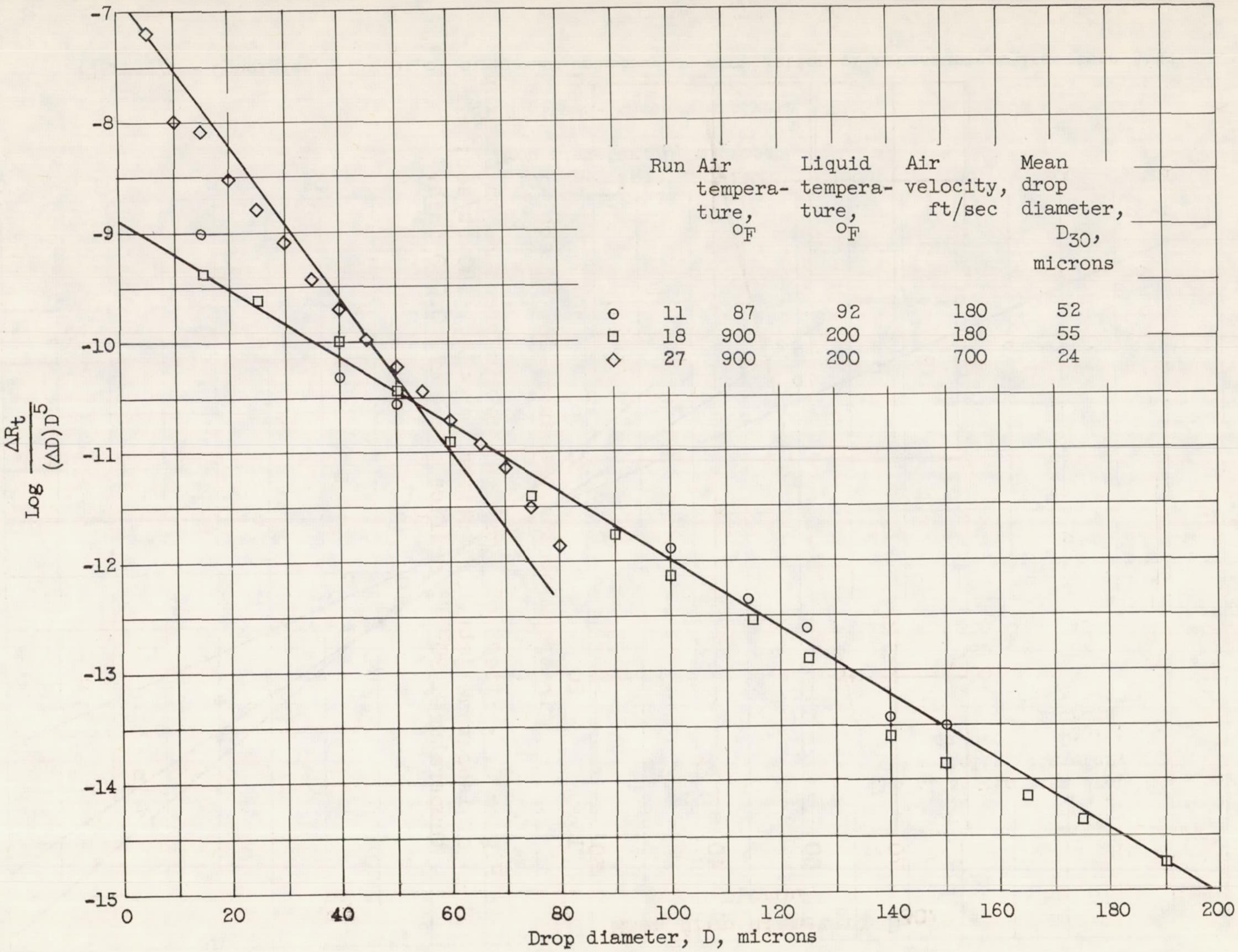

Figure 8. - Nukiyama-Tanasawa analysis showing combined effect of liquid and air temperature, and air velocity on atomization of crosscurrent isooctane jets.

4453

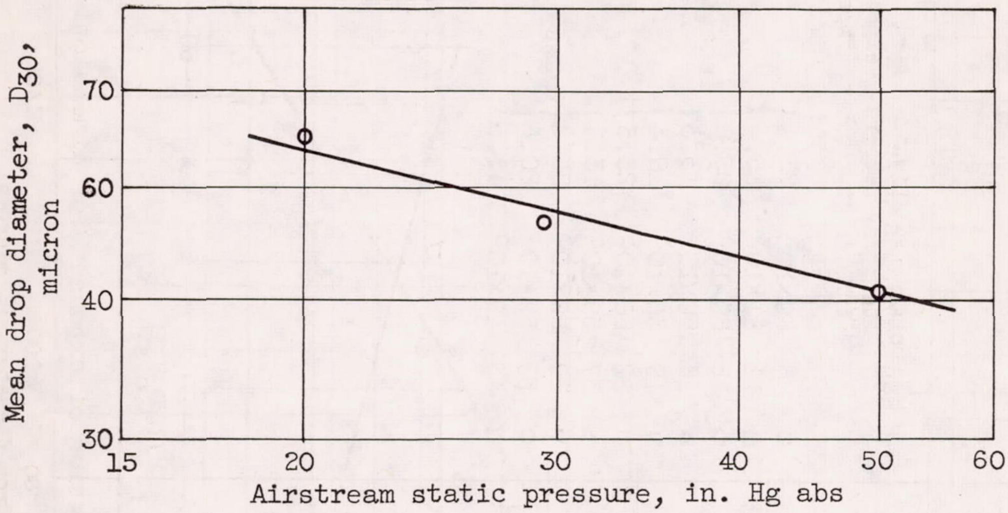

Figure 9. - Effect of airstream static pressure on breakup of isooctane jets. Airstream velocity, 180 ft/sec; air temperature, 90° F; orifice diameter, 0.030 inch.

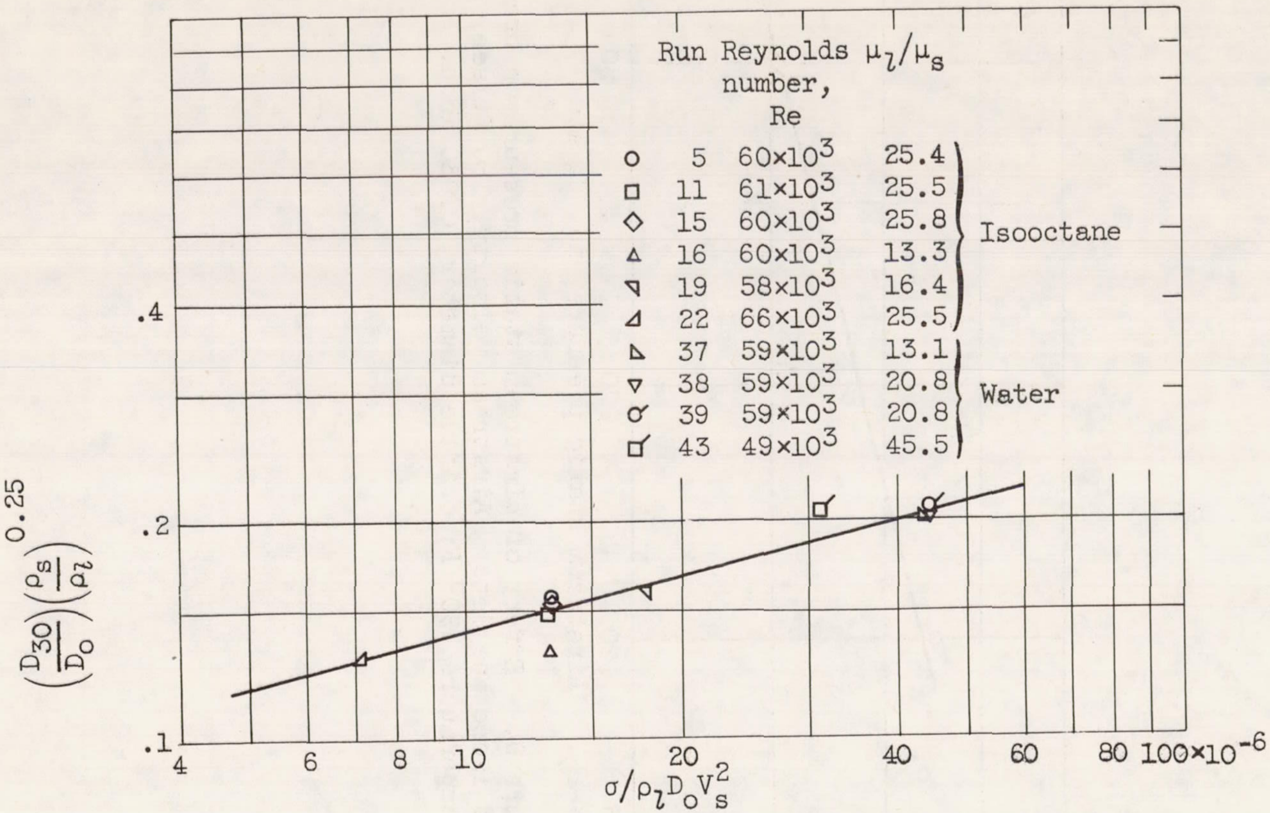

Figure 10. - Determination of exponent for dimensionless groups $\sigma/\rho_l D_o V_s^2$ and μ_l/μ_s.

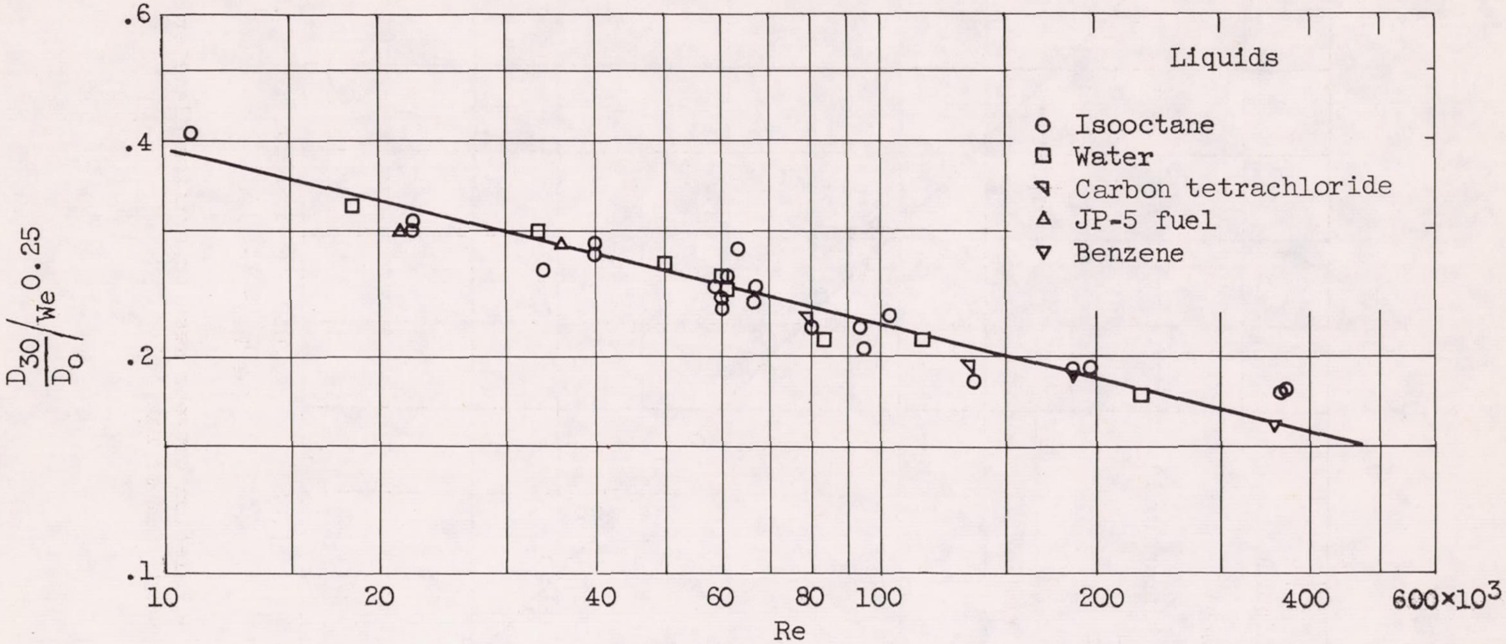

Figure 11. - Determination of Reynolds number exponent.

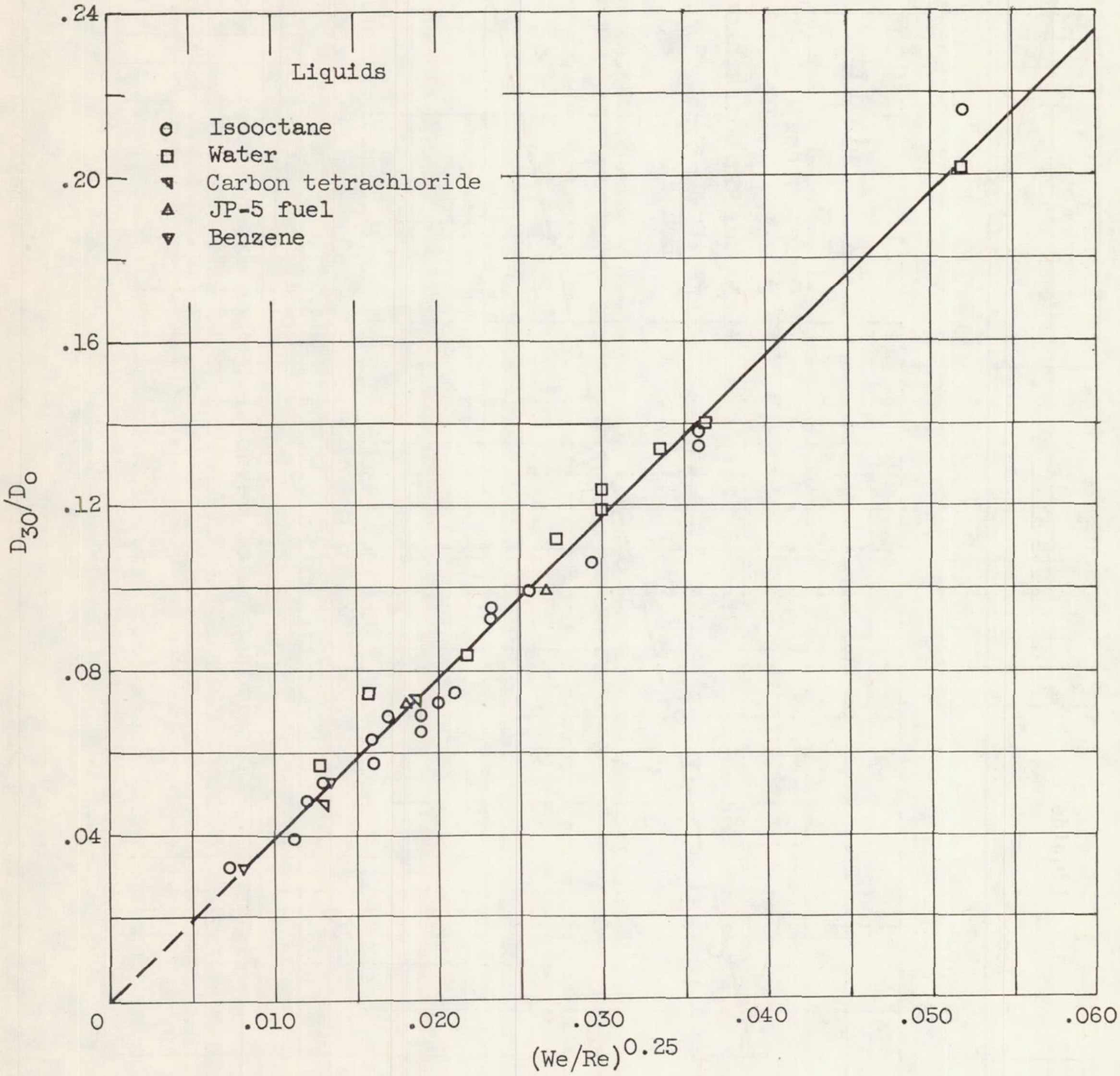

Figure 12. - Relation between mean to orifice diameter ratio and Weber-Reynolds number ratio.

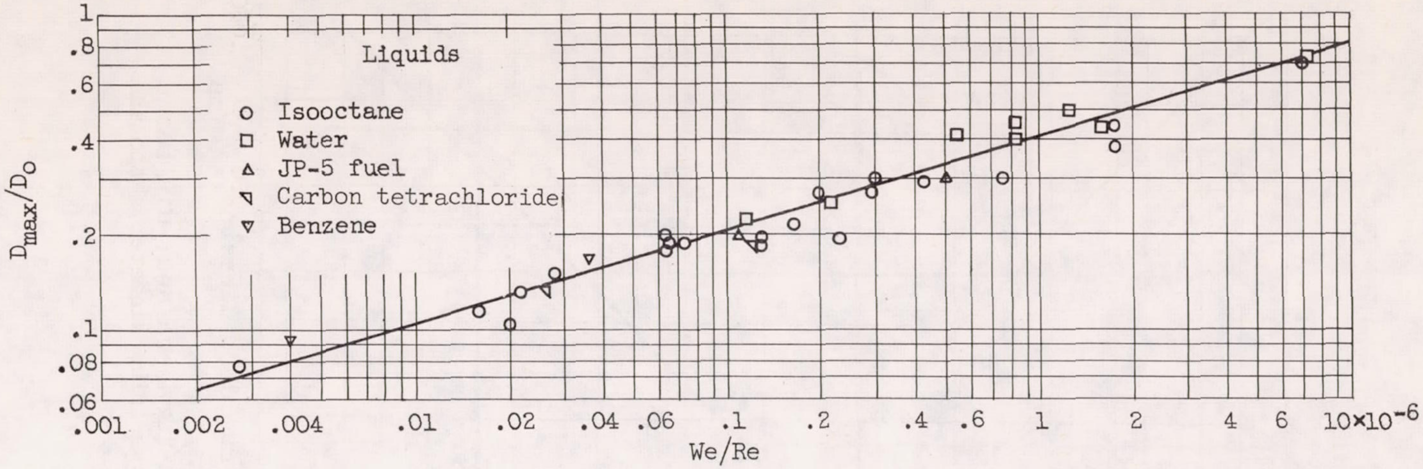

Figure 13. - Relation between maximum drop size to orifice-diameter ratio and Weber-Reynolds number ratio.

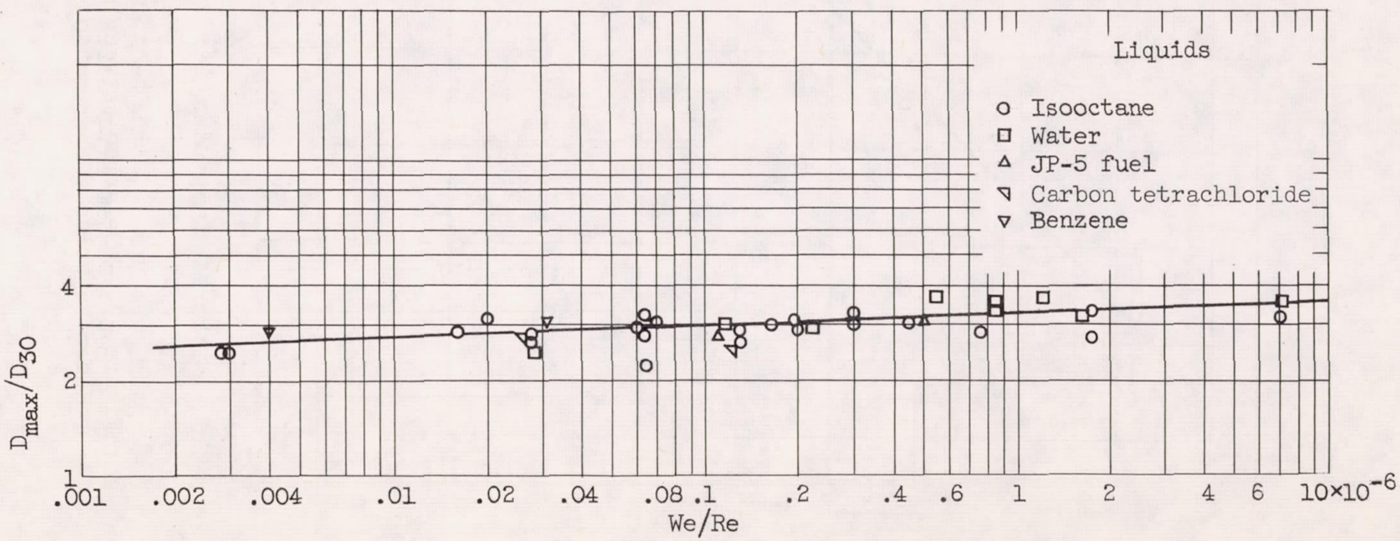

Figure 14. - Relation between maximum to mean drop-size ratio and Weber-Reynolds number ratio.

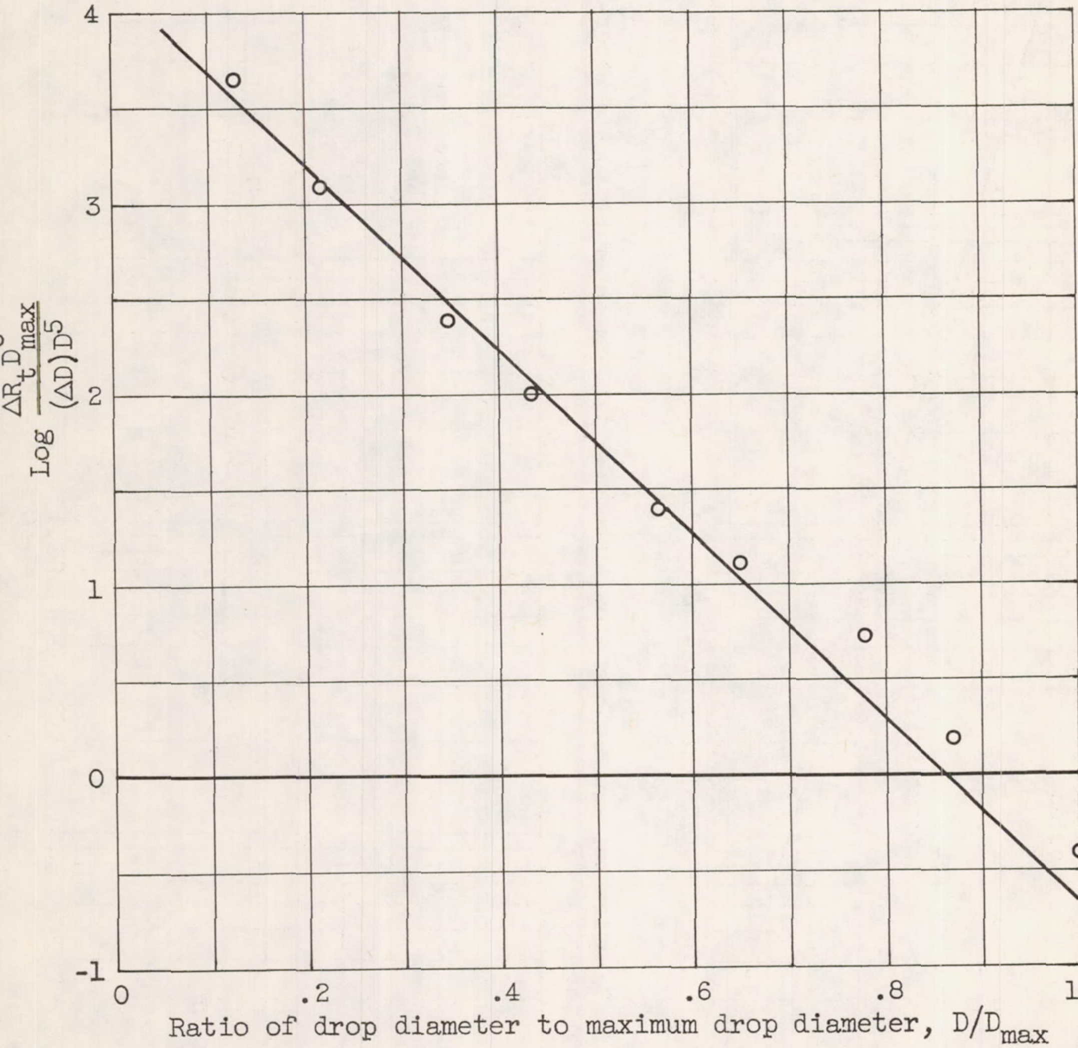

Figure 15. - Modified Nukiyama-Tanasawa analysis based on maximum drop size. Run 23.

NACA - Langley Field, Va.